Emodin azide methyl anthraquinone derivative triggers mitochondrial-dependent cell apoptosis involving in caspase-8-mediated Bid cleavage

Yanyan Yan,[1] Xiaodong Su,[2] Yongju Liang,[1] Jianye Zhang,[1] Chengjun Shi,[1] Yu Lu,[3] Lianquan Gu,[3] and Liwu Fu[1]

[1]State Key Laboratory of Oncology in South China and [2]Department of Thoracic Surgery, Cancer Center and [3]Department of Organic Chemistry, School of Chemistry and Chemical Engineering, Sun Yat-sen University, Guangzhou, People's Republic of China

Abstract

AMAD, an emodin azide methyl anthraquinone derivative, was extracted from the nature giant knotweed rhizome of traditional Chinese herbs. Here, we investigated the anticancer activities and signaling pathways implicated in AMAD-induced apoptosis in human breast cancer cell lines MDA-MB-453 and human lung adenocarcinoma Calu-3 cells. AMAD was found to have a potent cytotoxic effect on both cell lines. Hoechst 33258 staining and Annexin V/propidium iodide double staining exhibited the typical nuclear features of apoptosis and increased the proportion of apoptotic Annexin V–positive cells in a dose-dependent manner, respectively. Moreover, this apoptotic induction was associated with a collapse of the mitochondrial membrane potential and activated caspases (cysteine aspartase) cascade involving in caspase-8, caspase-9, caspase-3, and poly(ADP-ribose) polymerase cleavage in a concentration-dependent manner. It was noteworthy that AMAD also effectively cleaved Bid, a BH3 domain-containing proapoptotic Bcl-2 family member, and induced the subsequent release of cytochrome *c* from mitochondria into the cytosol. Furthermore, suppression of caspase-8 activity with Z-IETD-FMK partially inhibited release of cytochrome *c* and Bid cleavage induced by AMAD, whereas exposure to Z-LETD-FMK, a caspase-9 inhibitor, had no effect. Additionally, there was significant change in other mitochondrial membrane proteins triggered by AMAD, such as Bcl-xl and Bad. It was intriguing that AMAD decreased the generation of reactive oxygen species in both cell lines. DNA-binding assay exhibited apoptosis induced by AMAD was not involved in intercalating to DNA. Taken together, these data suggested that AMAD induced apoptosis via a mitochondrial pathway involving caspase-8/Bid activation in both cell lines. [Mol Cancer Ther 2008;7(6):1688–97]

Introduction

Apoptosis is a highly regulated and organized death process controlling the development and homeostasis of multicellular organisms. It is characterized by several well-defined processes including the decrease in cell volume, compaction of cytoplasmic organelles, condensation and fragmentation of nuclear chromatin, internucleosomal DNA cleavage, membrane blebbing, and activation of a family of cysteinyl aspartate-specific proteinases called caspase (1, 2). Two major pathways of apoptosis depending on different apoptotic stimuli are death receptor pathway (extrinsic) and mitochondrial pathway (intrinsic). In the extrinsic pathway, stimulation of death receptors such as Fas and tumor necrosis factor receptor 1 leads to clustering and formation of a death-inducing signaling complex, which includes the adapter protein, Fas-associated death domain, and initiator caspases such as caspase-8. Caspase-8 drives its activation through self-cleavage and then activates downstream caspases such as caspase-9 and caspase-3 (3). In the intrinsic pathway, death receptors transmit the death signals to mitochondria, resulting in the release of several mitochondrial intermembrane space proteins, such as cytochrome *c*, which associate with Apaf-1 and procaspase-9 to form the apoptosome (4).

The mitochondrial pathway is controlled and regulated by the Bcl-2 family proteins. The antiapoptotic subfamily comprises Bcl-2 and Bcl-xl. The multidomain proapoptotic subfamily consists of Bax and Bak and the BH3 domain-only proteins include Bid, Bad, and Bim (5). Proapoptotic and antiapoptotic Bcl-2 family members converge on mitochondria in response to the death signal and compete to regulate the release of cytochrome *c* (4). Bid, a BH3-only molecule of the Bcl-2 family, links death receptor signaling to the activation of apoptotic mechanisms in mitochondria. Death receptor–activated caspase-8 cleaves the Bid, which generates a truncated Bid fragment that collaborates with other proapoptotic proteins, such as Bax and Bak to promote the release of mitochondrial factors necessary for activation of executioner caspases and apoptosis.

Received 12/3/07; revised 3/14/08; accepted 4/3/08.

Grant support: 863 Key Project Foundation of China grant 2006AA09Z419 and National Natural Sciences Foundation of China grant 30672407.

The costs of publication of this article were defrayed in part by the payment of page charges. This article must therefore be hereby marked *advertisement* in accordance with 18 U.S.C. Section 1734 solely to indicate this fact.

Requests for reprints: Liwu Fu, State Key Laboratory of Oncology in South China, Cancer Center, Sun Yat-sen University, 651 Dongfeng Road East, Guangzhou 510060, People's Republic of China. Phone: 86-20-87343163; Fax: 86-20-87343170. E-mail: fulw@mail.sysu.edu.cn

doi:10.1158/1535-7163.MCT-07-2362

Anthraquinones represent a large family of compounds having diverse biological properties. Emodin (1,3,8-trihydroxy-6-methylanthraquinone) is a naturally occurring anthraquinone present in the roots and barks of numerous plants, molds, and lichens and an active ingredient of various Chinese herbs including *Rheum officinale* and *Polygonam cuspidatum* (6). Pharmacologic studies using crude as well as pure forms of emodin have been carried out so far and have indicated the role of emodin as purgative, antibacterial, immunosuppressive, vasorelaxant, cardiotonic, and hepatoprotective in nature (7, 8). Recent studies clearly revealed the specific activity of emodin in oncogene-stimulated cells of different origins as well as its utility of being used as a sensitizor of antitumor drug therapy (9–12). Additionally, because of its quinone structure, emodin may interfere with electron transport process and in altering cellular redox status, which may account for its cytotoxic properties in different systems.

We have reported the separation and structure identification of emodin azide methyl anthraquinone derivative (AMAD) as a new compound with a purity of >98%. It was obtained from modified structure of emodin extracted from the nature giant knotweed rhizome of traditional Chinese herbs. In this study, we deciphered the pathway of cell apoptosis induced by emodin AMAD and related molecular mechanisms.

Materials and Methods

Chemicals and Reagents

3-(4,5-Dimethylthiazol-2-yl)-2,5-diphenyltetrazolium bromide (MTT), 2′,7′-dichlorofluorescin diacetate, 3,3′-dihexyloxacarbocyanine iodide, and Hoechst 33258 were purchased from Sigma. Adriamycin was from ZhuHai MingZhi Pharmaceuticals. A selective inhibitor of caspase-8 (Z-IETD-FMK) and a caspase-9 inhibitor (Z-LETD-FMK) were purchased from R&D Systems. As a gift, pEGFPC2-H1-MDR1shDNA plasmid was obtained from Dr. Zhi Shi (Sun Yat-sen University). ApopNexin FITC Apoptosis Detection Kit was purchased from Chemicon. Antibodies against caspase-3, caspase-8, caspase-9, poly(ADP-ribose) polymerase (PARP), cytochrome *c*, Bcl-xl, and Bad were obtained from Cell Signaling Technology. Antibodies against Bax were purchased from Santa Cruz Biotechnology. Antibodies against glyceraldehyde-3-phosphate dehydrogenase, anti-mouse IgG-horseradish peroxidase, and anti-rabbit IgG-horseradish peroxidase were purchased from KangChen Biotechnology. All tissue culture supplies were purchased from Life Technologies. Other routine laboratory reagents were obtained from Whiga Biotechnology of analytical or high-performance liquid chromatography grade. Emodin AMAD with a purity of >98% was obtained from modified structure of emodin extracted from the nature giant knotweed rhizome of traditional Chinese herbs (Fig. 1B).

Cell Lines and Cell Culture

Human breast cancer cell lines MDA-MB-453, human lung adenocarcinoma Calu-3 cells, and normal mouse fibroblast NIH3T3 cell lines obtained from Cell Bank of Chinese Academy of Medical Sciences were grown in DMEM, MEM/nonessential amino acid, and RPMI 1640, respectively, which contain 100 units/mL penicillin, 100 μg/mL streptomycin, and 10% fetal bovine serum. All cells were cultured in a humidified atmosphere incubator of 5% CO_2 and 95% air at 37°C.

Cell Viability Assay

Cells were harvested during logarithmic growth phase and seeded in 96-well plates at a density of 3.5×10^4/mL in a final volume of 190 μL/well. After 24 h incubation, 10 μL AMAD full-range concentration was added to 96-well plates. After 68 h treatment, 10 μL MTT (10 mg/mL stock solution of saline) was added to each well for 4 h. Subsequently, the supernatant was removed, and MTT crystals were solubilized with 100 μL anhydrous DMSO each well. Thereafter, cell viability was measured by model 550 microplate reader (Bio-Rad) at 540 nm, with 655 nm as reference filter (13). The 50% inhibitory concentration (IC_{50}) was determined as the anticancer drug concentration

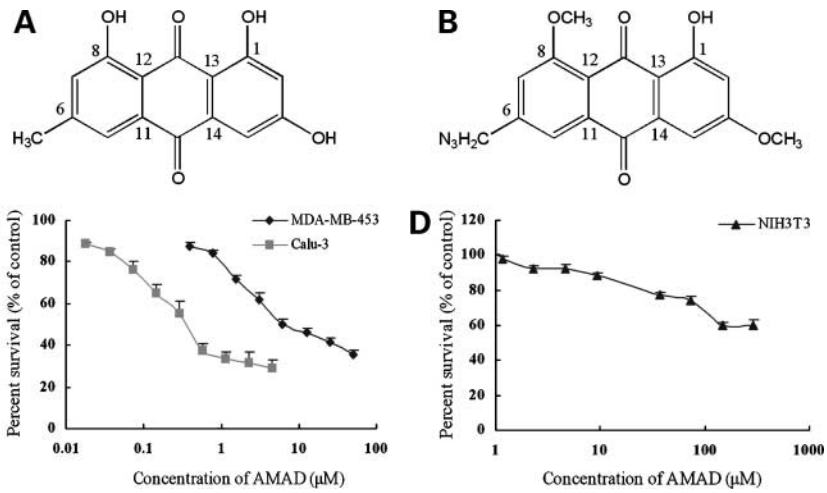

Figure 1. **A,** structure of emodin: 1,3,8-trihydroxy-6-methylanthraquinone. **B,** chemical structures of emodin AMAD: 6-nitrinemethyl-1-hydroxyl-3,8-diplmethoxyl-9,10-anthraquinone; molecular weight: 339.30. **C** and **D,** AMAD showed potent cytotoxicity to MDA-MB-453 and Calu-3 cells but had little cytotoxicity to normal mouse fibroblast NIH3T3 cells. Cytotoxicity was measured by MTT assay. The cells having grown for 24 h were exposed to a full range of concentrations of AMAD for 72 h. Cell viability was assessed by model 550 microplate reader after staining with MTT for 4 h. Mean ± SD of at least triplicate determinations. Each experiment was done in three replicate wells.

causing 50% reduction in cell viability and calculated from the cytotoxicity curves (Bliss' software). Cell percent survival was calculated using the following formula: survival (%) = [(mean experimental absorbance) / (mean control absorbance)] × 100%.

Assessment of Apoptosis Morphology by Hoechst 33258 Staining

After treatment with or without 2.30 to 9.20 μmol/L AMAD for MDA-MB-453 and 0.75 to 3 μmol/L AMAD for Calu-3, both floating and trypsinized adherent cells were collected, washed once with ice-cold PBS, fixed with 1 mL of 4% paraformaldehyde for 20 min, and washed once with ice-cold PBS. Then, the cells were incubated in 1 mL PBS containing 10 μmol/L Hoechst 33258 at 37°C for 30 min, washed twice, and observed using fluorescence microscopy with standard excitation filters (Leica Dmirb) in random microscopic fields at ×400 magnification (14).

Annexin V/Propidium Iodide Double-Staining Assay

Annexin V and propidium iodide (PI) staining was done using ApopNexin FITC Apoptosis Detection Kit. Cells (6×10^5) were seeded in 25 cm^2 flasks and allowed to attach for 24 h. After treated with the desired concentration AMAD for 48 h, both floating and attached cells were collected, washed with ice-cold PBS twice, and resuspended in 200 μL of 1× binding buffer containing Annexin V (1:50 according to the manufacturer's instruction) and 40 ng/sample PI for 15 min at 37°C in the dark (15). Then, the number of viable, apoptotic, and necrotic cells was quantified by flow cytometer (Becton Dickinson) and analyzed by the CellQuest software. Cells were excited at 488 nm and the emissions of Annexin V at 525 nm and PI were collected through 610 nm band-pass filters. At least 10,000 cells were analyzed for each sample. Percent apoptosis (%) = [(number of apoptotic cells) / (number of total cells observed)] × 100%.

DNA-Binding Assay

Being able to intercalate between nucleic bases, epirubicin was used as a positive control of DNA-binding assay (16). Briefly, 9 to 300 μmol/L AMAD or 5 to 160 μmol/L epirubicin was incubated with pEGFPC2-H1-MDR1shDNA at 37°C for 48 h; 150 μmol/L AMAD or 80 μmol/L epirubicin was incubated with pEGFPC2-H1-MDR1shDNA at 37°C for 1 to 48 h. Then, the mixture was electrophoresed on 1.2% agarose gel stained with 1.5 μmol/L EB at 60 V for 40 min in 0.5× TBE buffer [44.5 mmol/L Tris-boric acid and 1 mmol/L EDTA (pH 8.3)]. Analyses and photography were done with the gel imaging and analysis system (Vilber Lourmat; ref. 17).

Determination of Mitochondrial Membrane Potential

Mitochondrial membrane potential ($\Delta\Psi_m$) was measured by flow cytometry with the mitochondrial tracking fluorescent dye 3,3′-dihexyloxacarbocyanine iodide. The cationic lipophilic fluorochrome 3,3′-dihexyloxacarbocyanine iodide is a cell-permeable marker that specifically accumulates into mitochondrion depending on $\Delta\Psi_m$. After MDA-MB-453 and Calu-3 cells were exposed to 2.30 to 9.20 and 0.75 to 3 μmol/L AMAD for 48 h, respectively, 6×10^5 cells were harvested, centrifuged at 1,000 rpm for 5 min, and washed with ice-cold PBS once. Thereafter, cells were incubated with 40 nmol/L 3,3′-dihexyloxacarbocyanine iodide at 37°C for 20 min in the dark. Then, the cells were washed twice, resuspended in 1 mL PBS, and analyzed by FACS Calibur flow cytometer with the excitation wavelength of 484 nm and emission wavelength of 501 nm (16). At least 10,000 cells were determined for each sample. The data obtained from flow cytometry were analyzed by CellQuest software and expressed as mean fluorescence intensity. The expressed data were the results of at least three independent determinations.

Measurement of Reactive Oxygen Species Generation

2′,7′-Dichlorofluorescin diacetate is a fluorogenic freely permeable tracer specific for reactive oxygen species (ROS) assessment. It can be deacetylated by intracellular esterase to the nonfluorescent 2′,7′-dichlorofluorescin, which is oxidized by ROS to the fluorescent compound 2′,7′-dichloroflorescein. Thus, the fluorescence intensity of 2′,7′-dichloroflorescein is proportional to the amount of ROS produced by the cells. After MDA-MB-453 and Calu-3 cells were exposed to 2.30 to 9.20 and 0.75 to 3 μmol/L AMAD for 48 h, respectively, 6×10^5 cells were harvested, washed once with ice-cold PBS, and incubated with 50 μmol/L 2′,7′-dichlorofluorescin diacetate at 37°C for 20 min in the dark. Then, the cells were washed twice and maintained in 1 mL PBS. The ROS generation was assessed from 10,000 cells each sample by FACS Calibur flow cytometer at the excitation wavelength of 488 nm and emission wavelength of 530 nm (18). The data of 2′,7′-dichloroflorescein fluorescence intensity were evaluated by CellQuest software and expressed as mean fluorescence intensity. The experiment was done at least triplicate determination.

Whole-Cell Lysates and Western Blot Analysis

After MDA-MB-453 and Calu-3 cells were exposed to 2.30 to 9.20 and 0.75 to 3 μmol/L AMAD for 48 h, respectively [preincubated with Z-IETD-FMK (a caspase-8 inhibitor) or Z-LETD-FMK (a caspase-9 inhibitor)], whole cells were harvested and washed twice with ice-cold PBS, and the pellet was vortexed and 1× lysis buffer [50 mmol/L Tris-HCl (pH 6.8), 10% glycerol, 2% SDS, 0.25‰ bromophenol blue, and 0.1 mol/L DTT] was added for 100 μL/5×10^6 cells. After heated at 95°C for 20 min, the lysates were centrifuged at 12,000 rpm for 10 min and the supernatant was collected (19). The protein concentration was determined by nucleic acid-protein analyzer (Beckman). Equal amount of lysate protein was separated on 8% to 12% SDS-PAGE and transferred onto polyvinylidene difluoride membrane (Pall). The nonspecific binding sites were blocked with TBST buffer [150 mmol/L NaCl, 20 mmol/L Tris-HCl (pH 7.4), and 0.4% (v/v) Tween 20] containing 5% nonfat dry milk for 2 h. The membranes were incubated overnight at 4°C with specific primary antibodies. Then, the membranes were washed three times with TBST buffer and incubated at room temperature for 1 h with horseradish peroxidase–conjugated secondary antibody. After three washes with TBST buffer, the immunoblots were visualized by the enhanced Phototope-Horseradish Peroxidase Detection Kit

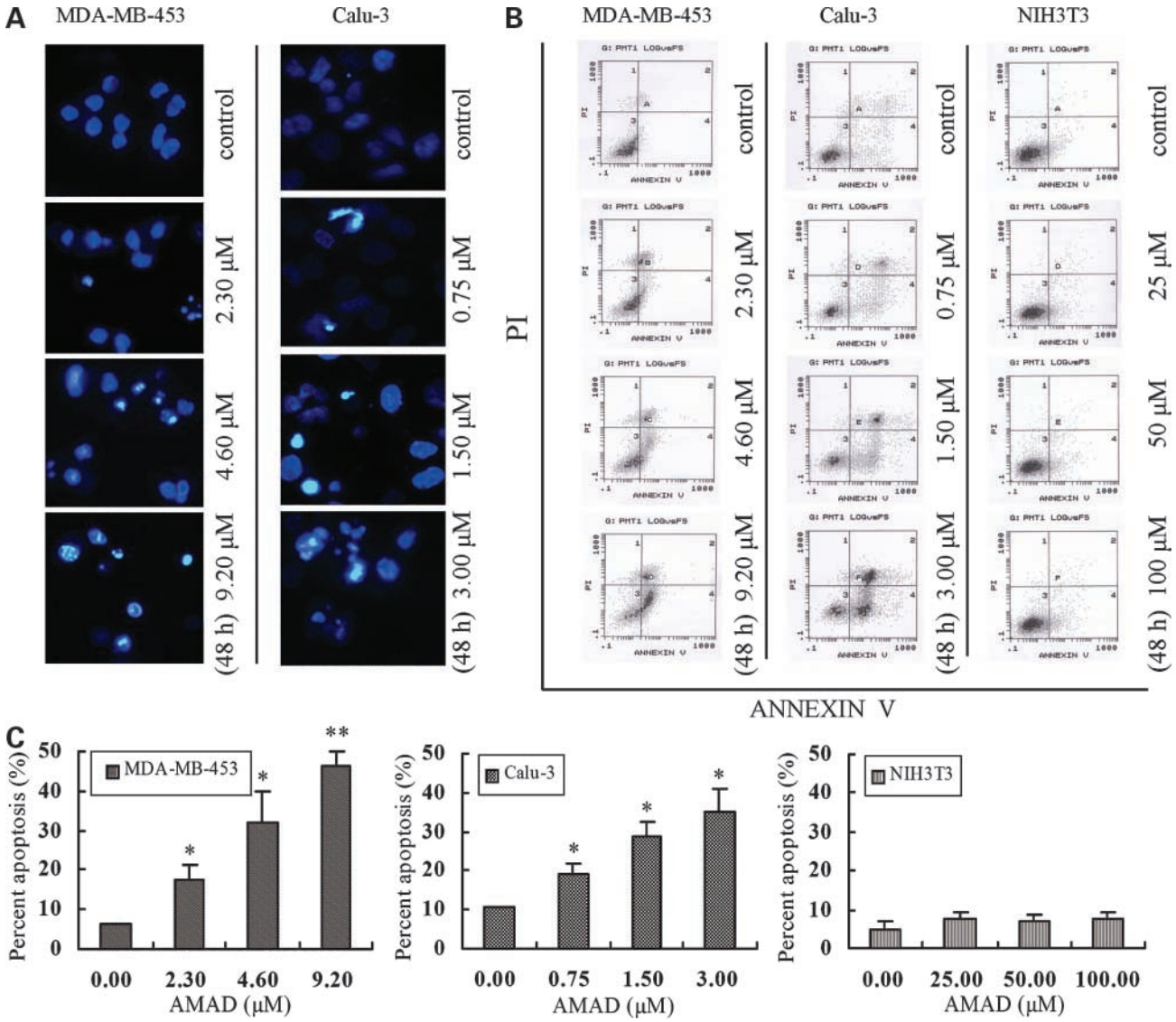

Figure 2. **A,** AMAD-mediated cell apoptosis morphologic changes were examined by Hoechst 33258 staining and observed under fluorescence microscope at ×400 magnification. MDA-MB-453 and Calu-3 cells were treated with 2.30 to 9.20 and 0.75 to 3 μmol/L AMAD for 48 h, respectively. The apoptotic cells detected by the fluorescence microscopy displayed condensed and fragmented nuclei, shrinkage of cell volume in a concentration-dependent manner. **B,** apoptosis analysis in MDA-MB-453, Calu-3, and NIH3T3 cells was assessed by Annexin V/PI double staining. After cells were exposed to three desired concentrations of AMAD for 48 h, respectively, the attached and detached cells were collected. Following staining with Annexin V and PI, cells were subjected to flow cytometer analysis. *Bottom right quadrant,* cells stained mainly by Annexin V (early apoptotic cells); *top right quadrant,* cells stained by both PI and Annexin V (late apoptotic/necrotic secondary necrosis); *top left quadrant,* cells stained mainly by PI viable cells; *bottom left quadrant,* cells negative for both Annexin V and PI. **C,** percent apoptosis. Early apoptotic cell population with Annexin V – positive but PI-negative cells increased gradually from 6.1% to 46.3% and from 10.7% to 35.1% in MDA-MB-453 and Calu-3 cells, respectively. However, AMAD had no obvious apoptosis-inducing effect on normal mouse fibroblast NIH3T3 cells even at the concentration of 100 μmol/L. Mean ± SD of three assays. *, $P < 0.05$; **, $P < 0.01$ versus control.

purchased from Cell Signaling Technology and exposed to Kodak medical X-ray processor (18).

Subcellular Fractionation for Western Blot Analysis of Cytosolic Cytochrome *c*

After MDA-MB-453 and Calu-3 cells were exposed to 2.30 to 9.20 and 0.75 to 3 μmol/L AMAD for 48 h, respectively [preincubated with Z-IETD-FMK (a caspase-8 inhibitor) or Z-LETD-FMK (a caspase-9 inhibitor)], whole cells were harvested by centrifugation at 1,000 rpm for 5 min. The pellets were washed twice with ice-cold PBS, suspended with 5-fold volume of ice-cold cell extract buffer [20 mmol/L 4-(2-hydroxyethyl)-1-piperazineethanesulfonic acid (HEPES-KOH; pH 7.5), 10 mmol/L KCl, 1.5 mmol/L $MgCl_2$, 1 mmol/L EDTA, 1 mmol/L EGTA, 1 mmol/L DTT, 250 mmol/L sucrose, 0.1 mmol/L phenylmethylsulfonyl fluoride, and 0.02 mmol/L aprotinin], and incubated for

40 min at 4°C. Then, the cells were centrifuged at 1,200 rpm for 10 min at 4°C; the supernatant was subsequently centrifuged at 12,000 rpm for 15 min at 4°C and the final supernatant was used as cytosolic fraction of cytochrome *c*. Then, 5× loading buffer [250 mmol/L Tris-HCl (pH 6.8), 50% (v/v) glycerol, 10% (w/v) SDS, 0.5% (w/v) bromphenol blue, and 5% (w/v) DTT] was added to the above obtained supernatant and the mixture was boiled at 100°C for 15 min. Thus, the protein solution was used for identification of cytosolic cytochrome *c* by Western blot with 15% SDS-PAGE and blotting onto polyvinylidene difluoride membrane. The cytochrome *c* protein was detected by using anti–cytochrome *c* antibody in the ratio of 1:1,000 (20).

Statistical Analysis

Results were done by *t* test or one-way ANOVA with SPSS 13.0 software. Data were presented as mean ± SD of at least triplicate determinations. *, $P < 0.05$ was indicative of significant difference and **, $P < 0.01$ was indicative of very significant difference.

Results

AMAD Exerted Potent Cytotoxicity against MDA-MB-453 and Calu-3 Cells

MTT assay measures the activity of mitochondrial dehydrogenase enzymes basing on its ability of cleaving tetrazolium ring to produce formazan; thus, the assay can be used as an index of cell viability. The cytotoxicity of AMAD to MDA-MB-453 and Calu-3 cells was measured by MTT assay. AMAD inhibited cell proliferation in a concentration-dependent manner in both MDA-MB-453 and Calu-3 cells after 72 h treatment (Fig. 1C). The IC_{50} of AMAD was 9.06 ± 0.95 μmol/L for MDA-MB-453 cells and 0.83 ± 0.21 μmol/L for Calu-3 cells, whereas for normal mouse fibroblast NIH3T3 cells was >100 μmol/L (Fig. 1D). The data suggested that AMAD exhibited potent cytotoxicity against MDA-MB-453 and Calu-3 cells but had little cytotoxicity to normal mouse fibroblast NIH3T3 cells.

AMAD Induced Apoptosis in MDA-MB-453 and Calu-3 Cells

To observe the morphologic characteristics of apoptosis, cells were stained with Hoechst 33258 after MDA-MB-453 and Calu-3 cells were exposed to 2.30 to 9.20 and 0.75 to 3 μmol/L AMAD for 48 h, respectively, and detected by the fluorescence microscopy. Control cells showed even distribution of the stain and round homogeneous nuclei feature. Apoptotic cells increased gradually in a dose-dependent manner and displayed typical changes including reduction of cellular volume, staining bright and condensed or fragmented nucleus (Fig. 2A). For a further assessment of apoptosis induced by AMAD, we examined the exposure of phosphatidylserine on the cell surface by using Annexin V/PI double staining. Flow cytometric analysis revealed that the percentage of apoptotic cells with Annexin V–positive but PI-negative cells increased gradually with concentration in AMAD-treated cells (Fig. 2B). The early percent apoptosis was 6.1 ± 0.5%, 17.3 ± 3.8%, 31.9 ± 7.9%, and 46.3 ± 3.6% in MDA-MB-453 cells and 10.7 ± 0.2%, 19.4 ± 2.4%, 28.8 ± 3.7%, and 35.1 ± 5.6% in Calu-3 cells, respectively (Fig. 2C). However, AMAD had no obvious apoptosis-inducing effect on normal mouse fibroblast NIH3T3 cells even at the concentration of 100 μmol/L (Fig. 2B and C).

DNA Intercalation Was Not Involved in Apoptosis Induced by AMAD

DNA is the acting target for some anticancer drugs such as Adriamycin, epirubicin, and daunomycin. We carried out the DNA-binding assay to investigate whether apoptosis induced by AMAD was related to intercalating to DNA as described in Materials and Methods. The results showed that epirubicin effectively intercalated to DNA in concentration-dependent manner. Importantly, it could intercalated to DNA after incubation with pEGFPC2-H1-MDR1shDNA at 37°C only for 1 h (Fig. 3). However, AMAD showed no binding to DNA even to very high concentration for a long time (Fig. 3). These results indicated that DNA intercalation was not involved in the apoptosis induced by AMAD.

AMAD Induced the Changes of $\Delta\Psi_m$ in MDA-MB-453 and Calu-3 Cells

3,3′-Dihexyloxacarbocyanine iodide was used as a mitochondrion-specific and voltage-dependent dye for determining $\Delta\Psi_m$, the loss of which is regarded as a limiting factor in the apoptotic pathway. To investigate the mechanisms via which AMAD induced apoptosis in MDA-MB-453 and Calu-3 cells, we determined the effect of AMAD on $\Delta\Psi_m$ by flow cytometric analysis. After cells were treated with AMAD as described above, the increase of $\Delta\Psi_m$ in concentration-dependent manner was observed in both cells (Fig. 4A and B, *top*). The levels of $\Delta\Psi_m$ were 122.0 ± 0.3%,

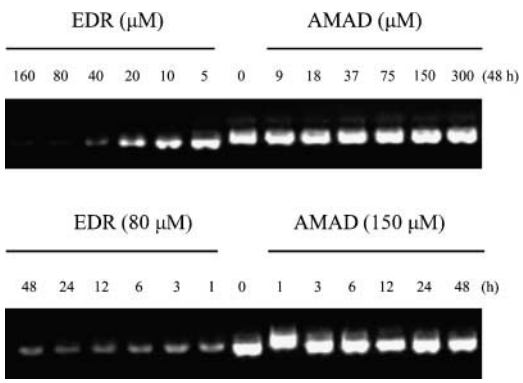

Figure 3. AMAD did not intercalate to DNA. After exposure, 9 to 300 μmol/L AMAD or 5 to 160 μmol/L epirubicin were incubated with pEGFPC2-H1-MDR1shDNA at 37°C for 48 h, respectively, and 150 μmol/L AMAD or 80 μmol/L epirubicin were incubated with pEGFPC2-H1-MDR1shDNA at 37°C for 1 to 48 h, respectively, DNA reaction mixtures was electrophoresed on 1.2% agarose gel stained with 1.5 μmol/L EB at 60 V for 40 min in 0.5× TBE buffer. The DNA bands were visualized under UV light and photographed. The DNA band fluorescence intensity of exposure to epirubicin was lower than the control in a concentration- and time-dependent manner and the DNA band fluorescence intensity of exposure to AMAD was no different from the control whatever concentration or time. Epirubicin was used as a positive control here.

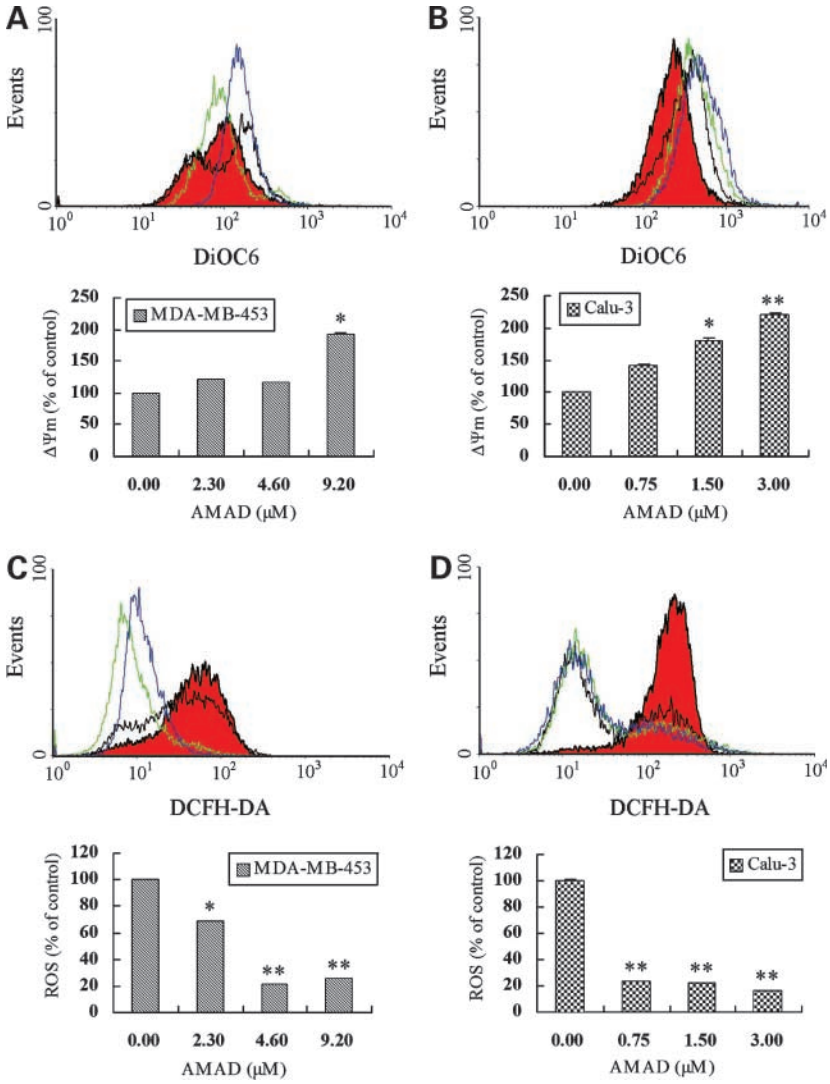

Figure 4. **A** and **B,** AMAD treatment resulted in the increase of $\Delta\Psi_m$. MDA-MB-453 and Calu-3 cells were exposed to 2.30 to 9.20 and 0.75 to 3 μmol/L AMAD for 48 h, respectively. The $\Delta\Psi_m$ was determined by flow cytometry. The $\Delta\Psi_m$ of both cell lines increased in a concentration-dependent manner. *Top,* changes of $\Delta\Psi_m$ in MDA-MB-453 and Calu-3 cells, respectively. *Red area* and *black, green*, and *blue lines,* $\Delta\Psi_m$ levels for control and 2.30, 4.60, and 9.20 μmol/L AMAD of MDA-MB-453 cells or for control and 0.75, 1.50, and 3 μmol/L AMAD of Calu-3 cells, respectively. *Bottom,* $\Delta\Psi_m$ levels of two cells, expressed as units of mean fluorescence intensity, were calculated as percentage of control. Mean ± SD of at least triplicate determinations. *, $P < 0.05$; **, $P < 0.01$ versus control. **C** and **D,** AMAD induced decrease of ROS generation in MDA-MB-453 and Calu-3 cells. After MDA-MB-453 and Calu-3 cells were exposed to 2.30 to 9.20 and 0.75 to 3 μmol/L AMAD for 48 h, respectively, intracellular ROS levels were analyzed by flow cytometry. Significant decreases of ROS production were observed after AMAD treatment in both cells. *Top,* ROS levels in MDA-MB-453 and Calu-3 cells, respectively. *Red area* and *black, green*, and *blue lines,* ROS levels for control and 2.30, 4.60, and 9.20 μmol/L AMAD of MDA-MB-453 cells or for control and 0.75, 1.50, and 3 μmol/L AMAD of Calu-3 cells, respectively. *Bottom,* ROS levels of two cells, expressed as units of mean fluorescence intensity, were calculated as percentage of control. Mean ± SD of at least triplicate determinations. *, $P < 0.05$; **, $P < 0.01$ versus control.

115.6 ± 0.2%, and 191.3 ± 3.4% of control in MDA-MB-453 cells and 142.7 ± 0.4%, 180.2 ± 5.8%, and 221.6 ± 1.7% of control in Calu-3 cells, respectively (Fig. 4A and B, *bottom*). The data suggested that mitochondrial dysfunction was involved in the apoptosis induced by AMAD.

Decrease of Intracellular ROS Level in MDA-MB-453 and Calu-3 Cells Induced by AMAD

To investigate whether the mitochondrial dysfunction was mediated by increase of ROS generation, we detected intracellular ROS level by flow cytometric method and 2′,7′-dichlorofluorescin diacetate was used as fluorescent probe. After MDA-MB-453 and Calu-3 cells were exposed to 2.30 to 9.20 and 0.75 to 3 μmol/L AMAD for 48 h, respectively, the decrease of ROS in concentration-dependent manner was observed in both cells (Fig. 4C and D, *top*). The intracellular ROS levels of control were 68.3 ± 0.4%, 20.4 ± 1.6%, and 25.7 ± 0.5% in MDA-MB-453 cells and 23.0 ± 0.2%, 22.1 ± 0.3%, and 15.9 ± 0.3% in Calu-3 cells, respectively (Fig. 4C and D, *bottom*). The results indicated that mitochondrial dysfunction was independent of more production of ROS.

Release of Cytochrome *c* and Activation of Caspases Were Involved in the Apoptosis Induced by AMAD

A variety of signaling pathways may be involved in apoptosis and mitochondrial pathway is one of the major apoptosis pathways. Release of cytochrome *c* from the mitochondria to cytosol is the limiting factor in mitochondrial pathway and the mitochondrial dysfunction has been suggested to cause the release of cytochrome *c*. Subsequently, it causes apoptosis by activation of caspase-9 in the presence of Apaf-1 and in turn results in the activation of downstream caspase-3, which can cleave PARP (21, 22). Additionally, Bcl-2 protein family and death receptor pathway are increasingly believed to have relationship with mitochondrial dysfunctions (23). To elucidate the interactions between the above apoptotic proteins, we detected the cytochrome *c* in cytosol, caspases, and other apoptotic related proteins of whole-cell lysates by Western

blot after MDA-MB-453 and Calu-3 cells were exposed to 2.30 to 9.20 and 0.75 to 3 μmol/L AMAD for 48 h, respectively. The results showed that the release of cytochrome *c* increased after treatment of AMAD in concentration-corresponding manner (Fig. 5A). Moreover, the activation of caspase-9 and caspase-3 and the cleavage of PARP in dose-dependent manner were observed. Additionally, AMAD could down-regulate the expression of Bcl-xl and up-regulate the expression of the Bad but did not influence the expression level of Bax. (Fig. 5B). Furthermore, activation of caspase-8 and cleavage of Bid were observed (Fig. 5C). These results revealed that death receptor pathway and mitochondrial apoptosis pathway were concomitantly involved in the apoptosis induced by AMAD in MDA-MB-453 and Calu-3 cells and the two pathways could be associated organically by Bid.

Release of Cytochrome *c* and Bid Cleavage Induced by AMAD Were Inhibited by Z-IETD-FMK rather than Z-LETD-FMK

It is increasingly believed that the cleavage form of Bid named as tBid caused by caspase-8 can lead to the release of cytochrome *c* from mitochondria into cytosol, which subsequently activates caspase-9. We carried out the caspase-8 inhibition experiments to clarify whether the activation of caspase-9 induced by AMAD was the downstream activation of caspase-8. After preincubation with 60 μmol/L Z-IETD-FMK or Z-LETD-FMK for 24 h, MDA-MB-453 or Calu-3 cells were treated with 4.60 or 3 μmol/L AMAD for 48 h, respectively. Then, the whole-cell lysates were analyzed by Western blot and corresponding antibodies. The results showed that suppression of caspase-8 activity with Z-IETD-FMK partially inhibited cell apoptosis (Fig. 6A), release of cytochrome *c* (Fig. 6B), and Bid cleavage induced by AMAD (Fig. 6C), whereas exposure to Z-LETD-FMK, a caspase-9 inhibitor, had no effect. Furthermore, both Z-IETD-FMK and Z-LETD-FMK could reduce PARP cleavage but fail to abolish the effects on other Bcl-2 family members triggered by AMAD, such as Bcl-xl and Bcl-2 (Fig. 6C).

Discussion

Cancer has become an increasing public health problem for its high rates of morbidity and mortality. In this study, we investigated the anticancer activity of AMAD belonging to emodin AMAD, which was extracted from the nature giant knotweed rhizome of traditional Chinese herbs. Considering that little is known about the anticancer activities and related mechanisms of it, we carried out further investigations to elucidate the antitumor activities of AMAD in human breast cancer cell lines MDA-MB-453 and human lung adenocarcinoma Calu-3 and the possible mechanisms involved.

Our experimental results showed that AMAD displayed potent cytotoxicity to MDA-MB-453 and Calu-3 cells and the IC_{50} was 9.06 and 0.83 μmol/L, respectively (Fig. 1C), whereas the IC_{50} of AMAD to normal mouse fibroblast NIH3T3 cells was >100 μmol/L (Fig. 1D). Apoptosis assay showed that apoptotic cells induced by AMAD displayed condensed and fragmented nuclei by Hoechst 33258 staining (Fig. 2A). Annexin V/PI double staining assay further confirmed the results of Hoechst 33258 staining by showing that the important membrane alterations relating to apoptosis in both cells and the percent apoptosis increased in dose-corresponding manner (Fig. 2B and C). However, AMAD had no obvious apoptosis-inducing effect on normal mouse fibroblast NIH3T3 cells even at the concentration of 100 μmol/L (Fig. 2B and C). Taken

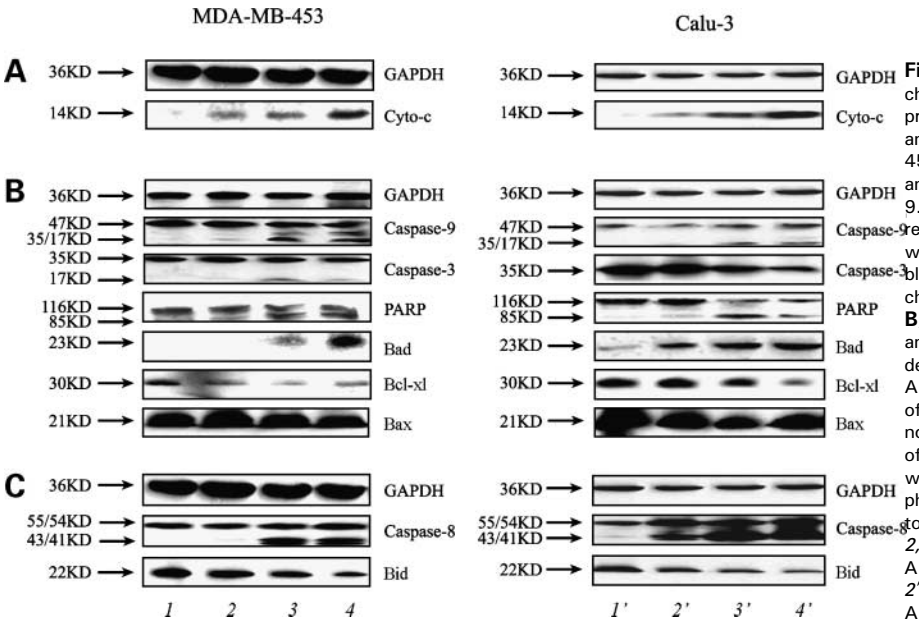

Figure 5. AMAD induced release of cytochrome *c* and changes of other apoptotic proteins related to mitochondrial pathway and death receptor pathway in MDA-MB-453 and Calu-3 cells. After MDA-MB-453 and Calu-3 cells were treated with 2.30 to 9.20 and 0.75 to 3 μmol/L AMAD for 48 h, respectively, the cytosolic fractions or the whole-cell lysates were assayed by Western blot and corresponding antibodies. **A,** mitochondrial cytochrome *c* release into cytosol. **B,** activations of caspase-9 and caspase-3 and the cleavage of PARP in dose-dependent manner were observed. Additionally, AMAD could down-regulate the expression of Bcl-xl and up-regulate that of Bad but did not influence the level of Bax. **C,** activations of caspase-8 and decrease of native Bid were observed. Glyceraldehyde-3-phosphate dehydrogenase detection was used to confirm equal protein loading. *1,* control; *2,* 2.30 μmol/L AMAD; *3,* 4.60 μmol/L AMAD; *4,* 9.20 μmol/L AMAD; *1′,* control; *2′,* 0.75 μmol/L AMAD; *3′,* 1.50 μmol/L AMAD; *4′,* 3 μmol/L AMAD.

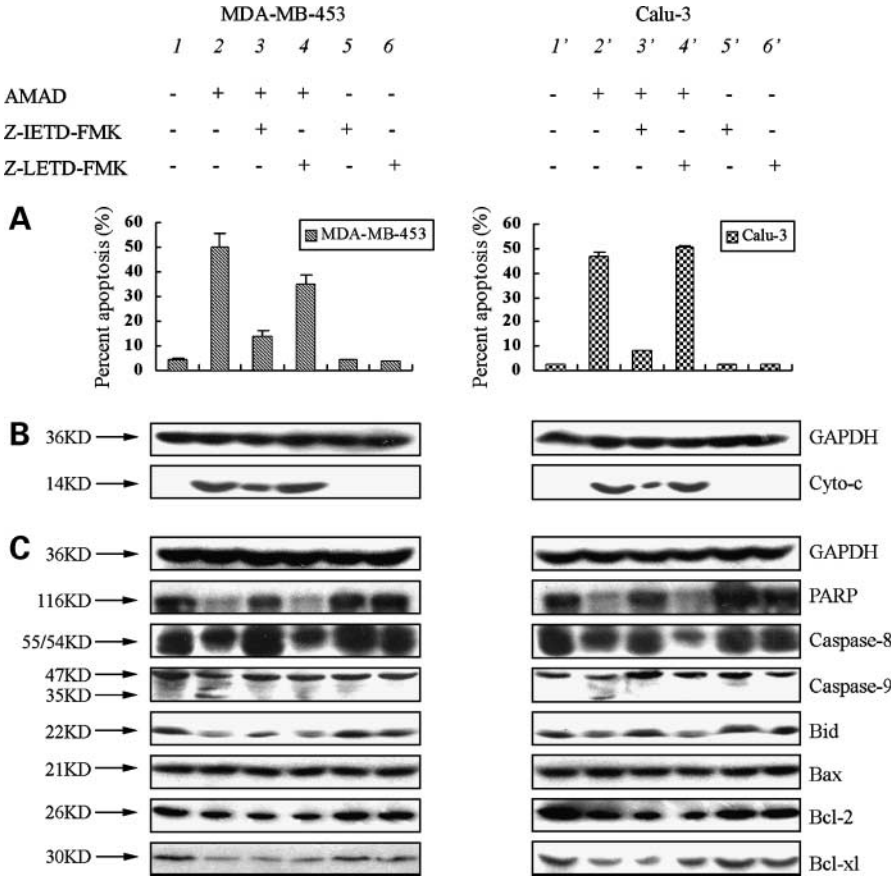

Figure 6. Cleavage of Bid (decrease of native Bid) and release of cytochrome *c* into cytosol induced by AMAD was inhibited by Z-IETD-FMK (a caspase-8 inhibitor) rather than Z-LETD-FMK (a caspase-9 inhibitor). After preincubation with 60 μmol/L Z-IETD-FMK or Z-LETD-FMK for 24 h, MDA-MB-453 cells or Calu-3 cells were treated with 4.60 or 3 μmol/L AMAD for 48 h, respectively. Then, the whole-cell lysates were assayed by Western blot and corresponding antibodies. **A,** percent apoptosis after exposure to inhibitors. **B,** release of cytochrome *c* into cytosol induced by AMAD was inhibited by Z-IETD-FMK rather than Z-LETD-FMK. **C,** Bid cleavage induced by AMAD was also inhibited by Z-IETD-FMK. Furthermore, both Z-IETD-FMK and Z-LETD-FMK could reduce PARP cleavage but did not restore the changes of other Bcl-2 family members triggered by AMAD, such as Bcl-xl and Bcl-2. Glyceraldehyde-3-phosphate dehydrogenase was detected to confirm equal protein loading. *1,* control; *2,* 4.60 μmol/L AMAD; *3,* 4.60 μmol/L AMAD + 60 μmol/L Z-IETD-FMK; *4,* 4.60 μmol/L AMAD + 60 μmol/L Z-LETD-FMK; *5,* 60 μmol/L Z-IETD-FMK; *6,* 60 μmol/L Z-LETD-FMK; *1′,* control; *2′,* 3 μmol/L AMAD; *3′,* 3 μmol/L AMAD + 60 μmol/L Z-IETD-FMK; *4′,* 3 μmol/L AMAD + 60 μmol/L Z-LETD-FMK; *5′,* 60 μmol/L Z-IETD-FMK; *6′,* 60 μmol/L Z-LETD-FMK.

together, these results suggested that AMAD indeed induced apoptosis in MDA-MB-453 and Calu-3 cells but had little cytotoxicity to normal mouse fibroblast NIH3T3 cells.

It has been reported that emodin induce apoptosis in many cells and in response to different stimuli. Proposed mechanisms for the proapoptotic effect include activation of caspases, induction of cytochrome *c* release, regulation of protein kinase C isoform expression, inhibition of NF-κB, and suppression of AP-1 (24). Consistent with a previous study, emodin AMAD induced apoptosis in MDA-MB-453 and Calu-3 cells. We carried out more investigations to illuminate the apoptotic pathways involved in the apoptosis induced by AMAD in both cells. Mitochondria has been suggested to play a key role in the regulation of apoptosis. Mitochondrial dysfunctions including loss of $\Delta\Psi_m$, permeability transition, and release of cytochrome *c* from mitochondria into cytosol are likely to cause apoptosis (25). In our research, the loss of $\Delta\Psi_m$ (Fig. 4A and B) and release of cytochrome *c* (Fig. 5A) were observed in AMAD-treated MDA-MB-453 and Calu-3 cells. Furthermore, the activation of caspase-8, caspase-9, and caspase-3, the cleavage of PARP, and changes of Bcl-2 family proteins (e.g. Bcl-xl/Bax and Bad) were detected by Western blot (Fig. 5B and C). Caspase-8 is one major enzyme activating caspase-3. Both TRAIL and tumor necrosis factor-α are known to bind to their cell surface receptors, leading to caspase-8 activation. Activated caspase-8 amplifies the apoptotic signal either by directly activating downstream caspases or by cleaving BH3 domain-only proteins such as Bid (26). In the current study, suppression of caspase-8 abrogated Bid cleavage, release of cytochrome *c* into cytosol, and subsequent apoptosis, suggesting that caspase-8 is required for AMAD-induced apoptosis and that the death receptor pathway (extrinsic) may be one possible mechanism for the proapoptotic effects of AMAD (Fig. 6A-C).

It is increasingly clear that Bid is the molecular linker bridging various death receptor pathways to the central mitochondria pathway (27). Bid relays the Fas/tumor necrosis factor apoptotic signal to the mitochondrial pathway (28) and is a specific substrate of caspase-8 in the Fas signaling pathway. Once Bid is cleaved by caspase-8, tBid translocates to the mitochondria from the cytosol to induce mitochondrial damage, cell shrinkage, nuclear condensation, and release of cytochrome *c*. In addition, tBid is able to activate Bax to form Bax multimers in the mitochondria (29), thereby inducing release of cytochrome *c*. It is noteworthy that Bid was cleaved after MDA-MB-453 and Calu-3 cells were treated with AMAD, showing decrease of native Bid protein (Fig. 5C). Furthermore, after treatment with Z-IETD-FMK rather than Z-LETD-FMK,

tBid formation was completely blocked, suggesting that Bid was the substrate of caspase-8 during apoptosis induced by AMAD in these cells (Fig. 6C). We also found that both Z-IETD-FMK and Z-LETD-FMK could reduce PARP cleavage but did not restore the changes of other Bcl-2 family members triggered by AMAD, such as Bcl-xl and Bcl-2 (Fig. 6C). Taken together, our results revealed that both intrinsic and extrinsic pathways took part in AMAD-induced apoptosis in two cell lines.

Recent studies have indicated that some anticancer agents (e.g., Adriamycin, epirubicin, and daunomycin) induce apoptosis in part with generation of ROS and the disruption of redox homeostasis (30). However, our research showed that AMAD suppressed production of ROS in MDA-MB-453 and Calu-3 cells (Fig. 4C and D). This indicated that apoptosis induced by AMAD was ROS independent. We tried to explain it chemically and biologically by comparing how analogues of AMAD influenced ROS generation. Emodin (or emodin-containing extracts) seems to accomplish an antioxidant status due to different mechanisms such as inhibition of radical formation, radical scavenging, inhibition of lipid peroxidation, and enhancement of antioxidant defenses (31–38). It is clear from the above studies that emodin behaves as a protector of cell constituents in presence of an oxidant stress. These findings provide supports for our result that AMAD decreased the ROS levels in MDA-MB-453 and Calu-3 cells. However, recent studies using emodin in cancer cells convey a different viewpoint (that emodin being a prooxidant) and are presently holding an upper hand. It is appropriate to speculate the expansion-ROS generation by emodin, considering the structural characteristics of emodin. It being a quinone and an effective electron acceptor is likely that emodin intracellularly interacts with molecular oxygen and generates superoxide anion (39). There are several recent studies showing the ability of emodin to generate ROS in a variety of tumor cells (40–45). However, reason for the earlier report of emodin not generating ROS in HL-60 leukemic cells is not clear (46). But it is a known fact that most prooxidants/antioxidants behave differently depending on the experimental conditions and is possible that such phenomenon works true for emodin as well. This may also reflect more when cell lines of different tissue origin are used for analysis; it is known that cells vary with respect to their antioxidant status.

As we know, DNA still remains an attractive target for the design of antitumor agents (47). Anthracyclines belong to the most useful antitumor drugs ever developed and the mechanism of intercalating to DNA has been studied extensively. Epirubicin, a type of anthracyclines, exerts its antitumor effect by intercalating to DNA. Anthraquinone derivative also contained anthracycline. To clarify whether AMAD showed cytotoxicity to MDA-MB-453 and Calu-3 cells via DNA-targeted pathway, we carried out the DNA-binding assay. In this study, epirubicin could compete with EB, a well-known DNA intercalator, to intercalate to DNA and the decreases of DNA bands fluorescence intensity exposed to epirubicin were observed. However, there were no dramatic differences of the DNA band fluorescence intensity between treatment with AMAD and the control (Fig. 3). The results showed that AMAD-induced apoptosis might not involve intercalating to DNA.

In summary, AMAD was a potent cytotoxic agent to MDA-MB-453 and Calu-3 cells. Cross-talk between the caspase-8/Bid pathway and the mitochondrial pathway may exist in AMAD-induced apoptosis. Moreover, the mitochondrial pathway was independent of generation of ROS. DNA-binding assay implied that intercalating to DNA was not involved in apoptosis induced by AMAD. Our results revealed that AMAD may be a promising compound opening better anticancer treatment options.

Disclosure of Potential Conflicts of Interest

No potential conflicts of interest were disclosed.

Acknowledgments

We thank Dr. Zhi Shi for kindly providing pEGFPC2-H1-MDR1shDNA plasmid and Drs. Liming Chen and Chunling Dai for critically reading this article.

References

1. Fesik SW. Promoting apoptosis as a strategy for cancer drug discovery. Nat Rev Cancer 2005;5:876–85.

2. Strasser A, O'Connor L, Dixit VM. Apoptosis signaling. Annu Rev Biochem 2000;69:217–45.

3. Ashkenazi A, Dixit VM. Death receptors: signaling and modulation. Science 1998;281:1305–8.

4. Hengartner MO. The biochemistry of apoptosis. Nature 2000;407:770–6.

5. Tsujimoto Y. Cell death regulation by the Bcl-2 protein family in the mitochondria. J Cell Physiol 2003;195:158–67.

6. Demirezer LO, Kuruüzüm-Uz A, Bergere I, Schiewe HJ, Zeeck A. The structures of antioxidant and cytotoxic agents from natural source: anthraquinones and tannins from roots of *Rumex patientia*. Phytochemistry 2001;58:1213–7.

7. Yagi T, Yamauchi K. Synergistic effects of anthraquinones on the purgative activity of rhein anthrone in mice. J Pharm Pharmacol 1999;51:93–5.

8. Matsuda H, Shimoda H, Morikawa T, Yoshikawa M. Phytoestrogens from the roots of *Polygonum cuspidatum* (Polygonaceae): structure-requirement of hydroxyanthraquinones for estrogenic activity. Bioorg Med Chem Lett 2001;11:1839–42.

9. Zhang L, Chang CJ, Bacus SS, Hung MC. Suppressed transformation and induced differentiation of HER-2/*neu*-overexpressing breast cancer cells by emodin. Cancer Res 1995;55:3890–6.

10. Zhang L, Hung MC. Sensitization of HER-2/*neu*-overexpressing non-small cell lung cancer cells to chemotherapeutic drugs by tyrosine kinase inhibitor emodin. Oncogene 1996;12:571–6.

11. Zhang L, Lau YK, Xi L, et al. Tyrosine kinase inhibitors, emodin and its derivative repress HER-2/*neu*-induced cellular transformation and metastasis-associated properties. Oncogene 1998;16:2855–63.

12. Zhang L, Lau YK, Xia W, Hortobagyi GN, Hung MC. Tyrosine kinase inhibitor emodin suppresses growth of HER-2/*neu*-overexpressing breast cancer cells in athymic mice and sensitizes these cells to the inhibitory effect of paclitaxel. Clin Cancer Res 1999;5:343–53.

13. Chen LM, Wu XP, Ruan JW, et al. Screening novel, potent multidrug-resistant modulators from imidazole derivatives. Oncol Res 2004;14:355–62.

14. Wu QL, Wu XP, Liang YJ, Chen LM, Ding Y, Fu LW. P-glycoprotein is not involved in pathway of anti-Fas/Fas-induced apoptosis in KBv200 cells. World J Gastroenterol 2005;11:3544–8.

15. Sewell JM, Mayer I, Langdon SP, Smyth JF, Jodrell DI, Guichard SM.

The mechanism of action of Kahalalide F: variable cell permeability in human hepatoma cell lines. Eur J Cancer 2005;41:1637 – 44.

16. Wang X-H, Jia D-Z, Liang Y-J, et al. Lgf-YL-9 induces apoptosis in human epidermoid carcinoma KB cells and multidrug resistant KBv200 cells via reactive oxygen species-independent mitochondrial pathway. Cancer Lett 2007;249:256 – 70.

17. Matsuba Y, Edatsugi H, Mita I, Matsunaga A, Nakanishi O. A novel synthetic DNA minor groove binder, MS-247: antitumor activity and cytotoxic mechanism. Cancer Chemother Pharmacol 2000;46:1 – 9.

18. Zhang JY, Wu HY, Xia XK, et al. Anthracenedione derivative 1403P-3 induces apoptosis in KB and KBv200 cells via reactive oxygen species-independent mitochondrial pathway and death receptor pathway. Cancer Biol Ther 2007;6:1413 – 21.

19. Rubio S, Quintana J, López M, Eiroa JL, Triana J, Estévez F. Phenylbenzopyrones structure-activity studies identify betuletol derivatives as potential antitumoral agents. Eur J Pharmacol 2006;548:9 – 20.

20. Lin S, Fujii M, Hou DX. Rhein induces apoptosis in HL-60 cells via reactive oxygen species-independent mitochondrial death pathway. Arch Biochem Biophys 2003;418:99 – 107.

21. Barry M, Heibein JA, Pinkoski MJ, et al. Granzyme B short-circuits the need for caspase 8 activity during granule-mediated cytotoxic T-lymphocyte killing by directly cleaving Bid. Mol Cell Biol 2000;20: 3781 – 94.

22. Nakagawa T, Zhu H, Morishima N, et al. Caspase-12 mediates endoplasmic-reticulum-specific apoptosis and cytotoxicity by amyloid-β. Nature 2000;403:98 – 103.

23. Lavrik IN, Golks A, Baumann S, Krammer PH. Caspase-2 is activated at the CD95 death-inducing signaling complex in the course of CD95-induced apoptosis. Blood 2006;108:559 – 65.

24. Srinivas G, Babykutty S, Sathiadevan PP, Srinivas P. Molecular mechanism of emodin action: transition from laxative ingredient to an antitumor agent. Med Res Rev 2007;27:591 – 608.

25. Wang Y, Perchellet EM, Tamura M, Hua DH, Perchellet JP. Induction of poly(ADP-ribose) polymerase-1 cleavage by antitumor triptycene bisquinones in wild-type and daunorubicin-resistant HL-60 cell lines. Cancer Lett 2002;188:73 – 83.

26. Kruidering M, Evan GI. Caspase-8 in apoptosis: the beginning of ''the end''? IUBMB Life 2000;50:85 – 90.

27. Yin XM. Bid, a BH3-only multi-functional molecule, is at the cross road of life and death. Gene 2006;369:7 – 19.

28. Chou JJ, Li H, Salvesen GS, Yuan J, Wagner G. Solution structure of BID, an intracellular amplifier of apoptotic signaling. Cell 1999;96: 615 – 24.

29. Roucou X, Montessuit S, Antonsson B, Martinou JC. Bax oligomerization in mitochondrial membranes requires tBid (caspase-8-cleaved Bid) and a mitochondrial protein. Biochem J 2002;368:915 – 21.

30. Xia Z, Lundgren B, Bergstrand A, DePierre JW, Nassberger L. Changes in the generation of reactive oxygen species and in mitochondrial membrane potential during apoptosis induced by the antidepressants imipramine, clomipramine, and citalopram and the effects on these changes by Bcl-2 and Bcl-X(L). Biochem Pharmacol 1999;57:1199 – 208.

31. Sato M, Maulik G, Bagchi D, Das DK. Myocardial protection by protykin, a novel extract of *trans*-resveratrol and emodin. Free Radic Res 2000;32:135 – 44.

32. Yim TK, Wu WK, Mak DH, Ko KM. Myocardial protective effect of an anthraquinone-containing extract of *Polygonum multiflorum ex vivo*. Planta Med 1998;64:607 – 11.

33. Huang SS, Yeh SF, Hong CY. Effect of anthraquinone derivatives on lipid peroxidation in rat heart mitochondria: structure-activity relationship. J Nat Prod 1995;58:1365 – 71.

34. Choi JS, Chung HY, Jung HA, Park HJ, Yokozawa T. Comparative evaluation of antioxidant potential of alaternin (2-hydroxyemodin) and emodin. J Agric Food Chem 2000;48:6347 – 51.

35. Chiu PY, Mak DH, Poon MK, Ko KM. *In vivo* antioxidant action of a lignan-enriched extract of *Schisandra* fruit and an anthraquinone-containing extract of *Polygonum* root in comparison with schisandrin B and emodin. Planta Med 2002;68:951 – 6.

36. Du Y, Ko KM. Effects of emodin treatment on mitochondrial ATP generation capacity and antioxidant components as well as susceptibility to ischemia-reperfusion injury in rat hearts: single versus multiple doses and gender difference. Life Sci 2005;77:2770 – 82.

37. Ng TB, Liu F, Lu Y, Cheng CH, Wang Z. Antioxidant activity of compounds from the medicinal herb *Aster tataricus*. Comp Biochem Physiol C Toxicol Pharmacol 2003;136:109 – 15.

38. Jung HA, Chung HY, Yokozawa T, Kim YC, Hyun SK, Choi JS. Alaternin and emodin with hydroxyl radical inhibitory and/or scavenging activities and hepatoprotective activity on tacrine-induced cytotoxicity in HepG2 cells. Arch Pharm Res 2004;27:947 – 53.

39. Rahimipour S, Bilkis I, Peron V, et al. Generation of free radicals by emodic acid and its [D-Lys^6]GnRH-conjugate. Photochem Photobiol 2001; 74:226 – 36.

40. Wang XJ, Yang J, Cang H, Zou YQ, Yi J. Gene expression alteration during redox-dependent enhancement of arsenic cytotoxicity by emodin in HeLa cells. Cell Res 2005;15:511 – 22.

41. Su YT, Chang HL, Shyue SK, Hsu SL. Emodin induces apoptosis in human lung adenocarcinoma cells through a reactive oxygen species-dependent mitochondrial signaling pathway. Biochem Pharmacol 2005; 70:229 – 41.

42. Yi J, Yang J, He R, et al. Emodin enhances arsenic trioxide-induced apoptosis via generation of reactive oxygen species and inhibition of survival signaling. Cancer Res 2004;64:108 – 16.

43. Yang J, Li H, Chen YY, et al. Anthraquinones sensitize tumor cells to arsenic cytotoxicity *in vitro* and *in vivo* via reactive oxygen species-mediated dual regulation of apoptosis. Free Radic Biol Med 2004;37: 2027 – 41.

44. Jing YW, Yi J, Chen YY, et al. Dicoumarol alters cellular redox state and inhibits nuclear factor κB to enhance arsenic trioxide-induced apoptosis. Acta Biochim Biophys Sin (Shanghai) 2004;36:235 – 42.

45. Jing X, Ueki N, Cheng J, Imanishi H, Hada T. Induction of apoptosis in hepatocellular carcinoma cell lines by emodin. Jpn J Cancer Res 2002;93: 874 – 82.

46. Chen YC, Shen SC, Lee WR, et al. Emodin induces apoptosis in human promyeloleukemic HL-60 cells accompanied by activation of caspase 3 cascade but independent of reactive oxygen species production. Biochem Pharmacol 2002;64:1713 – 24.

47. Dias N, Jacquemard U, Baldeyrou B, et al. Synthesis of 2,6-diphenylpyrazine derivatives and their DNA binding and cytotoxic properties. Eur J Med Chem 2005;40:1206 – 13.

Molecular Cancer Therapeutics

Emodin azide methyl anthraquinone derivative triggers mitochondrial-dependent cell apoptosis involving in caspase-8-mediated Bid cleavage

Yanyan Yan, Xiaodong Su, Yongju Liang, et al.

Mol Cancer Ther 2008;7:1688-1697.